Journal Name

ARTICLE

Photocatalytic hydrogen evolution with ruthenium polypyridine sensitizers: Unveiling the key factors to improve efficiencies.

Received 00th January 20xx,
Accepted 00th January 20xx

DOI: 10.1039/x0xx00000x

www.rsc.org/

Elisa Deponti and Mirco Natali*

Photochemical hydrogen evolution studies aimed at evaluating new molecular catalysts have usually exploited $Ru(bpy)_3^{2+}$ (where bpy = 2,2'-bipyridine) as the photosensitizer of reference, thanks to its suitable optical and redox properties. In principle, an additional improvement of the photocatalytic performances can be achieved also by a careful adjustement of the photophysical and/or electrochemical characteristics of the ruthenium-based sensitizer. Herein we describe homogenous molecular systems for photocatalytic hydrogen evolution composed of a series of ruthenium polypyridine complexes as the photosensitizers (**Ru1-4**), a cobaloxime catalyst, and ascorbic acid as the sacrificial electron donor. Suitable functionalizations of the 4,4' positions of the bipyridine ligands have been addressed in order to modify the redox properties of the chromophores rather than their optical ones. A careful and detailed kinetic characterization of the relevant processes at the basis of the hydrogen evolving photocatalysis have been addressed to rationalize the observed behavior. The results show that the ruthenium complex involving two 2,2'-bipyridines and one 4,4'-dimethyl-2,2'-bipyridine (**Ru2**), may outperform the standard $Ru(bpy)_3^{2+}$ (**Ru1**), combining the right balance of structural and redox properties, thus posing as an alternative benchmark photosensitizer for the study of new hydrogen evolving catalysts.

Introduction

It is well established that hydrogen generation via solar driven water splitting (artificial photosynthesis) represents one of the major goals for the production of clean fuels for a sustainable development.[1] In the last years, large efforts have been thus devoted to the preparation and characterization of photocatalytic systems capable of accomplishing this task at both the heterogeneous and homogeneous level.[2] Homogenous systems for hydrogen production are composed of at least three molecular components, namely a photosensitizer, a catalyst, and a sacrificial electron donor.[3,4] In a three-component system of this kind reduction of the catalyst to drive hydrogen production can take place by two different photochemical routes (Scheme 1): (i) an *oxidative* mechanism, whereby excitation of the photosensitizer is followed by oxidative quenching by the catalyst and the oxidized sensitizer is then reduced by the sacrificial agent (Scheme 1a), and (ii) a *reductive* mechanism, involving first reaction of the excited sensitizer with the sacrificial donor yielding a photogenerated reducing agent which transfers an electron to the catalyst (Scheme 1b). In both cases, once oxidized, the sacrificial electron donor undergoes decomposition thus avoiding detrimental charge recombination processes to occur. After the first photochemical cycle is completed and an electron permanently resides at the catalytic center, a new photochemical cycle takes place, following either pathway (i) or (ii), yielding a doubly reduced species of the catalyst potentially capable of hydrogen production. In the absence of any particular interactions between each molecular components, the kinetic competition between the oxidative quenching of the sensitizer by the catalyst and the reductive quenching by the donor directly determines the actual photochemical mechanism.

As far as the light-harvesting component within the aforementioned photochemical system is concerned, a large

Scheme 1. Schematic representation of photoinduced catalyst reduction within a three-component system: (a) *oxidative* and (b) *reductive* mechanism. Abbreviations: P = photosensitizer, HEC = hydrogen evolving catalyst, and SD = sacrificial electron donor.

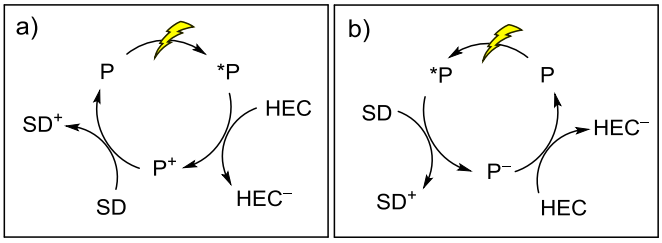

Dipartimento di Scienze Chimiche e Farmaceutiche, Università degli Studi di Ferrara, via Fossato di Mortara 17-19, and Centro Interuniversitario per la Conversione Chimica dell'Energia Solare (SOLARCHEM), sez. di Ferrara, via L. Borsari 46, 44121 Ferrara, Italy.

Electronic Supplementary Information (ESI) available: Steady-state and time-resolved emission data for quenching of **Ru1-4** complexes by **AscH**; second-order kinetic analyses of charge recombination between reduced sensitizer and oxidized sacrificial donor; Stern-Volmer plots of quenching of excited **Ru1-4** by **CoDMG**; laser flash photolysis experiments on **Ru2-4** in the presence of **CoDMG**; estimation of the bimolecular rate constants for electron transfer from the reduced sensitizer to the catalyst; cyclic voltammetry and absorption spectra of **CoDMG** with and without **AscH**; comparison of absorption spectra before and after the photocatalytic hydrogen evolution experiments. See DOI: 10.1039/x0xx00000x

amount of experimental studies aiming at investigating new catalysts and optimizing their photocatalytic performances has exploited the well-known $Ru(bpy)_3^{2+}$ chromophore (where bpy = 2,2'-bipyridine) as the photosensitizer.[5-8] The reasons at the basis of this choice have been mainly dictated by the following properties: (a) strong absorption in the visible, (b) excited-state lifetime appropriate for intermolecular processes, (c) excited-state redox potentials to favor both reduction of the catalyst (*oxidative* mechanism, Scheme 1a) and oxidation of the sacrificial agent (*reductive* mechanism, Scheme 1b), (d) sufficient redox potentials of the $Ru(bpy)_3^{3+}$ oxidized species and the $Ru(bpy)_3^{+}$ reduced species to react with most of the sacrificial donors used (*oxidative* mechanism, Scheme 1a) or with most of the catalysts (*reductive* mechanism, Scheme 1b), respectively.[9]

To this respect, while attention has been paid to the development and characterization of new molecular catalysts taking advantage of $Ru(bpy)_3^{2+}$ as the light-harvesting photosensitizer, little consideration has been given to the ruthenium-based sensitizer in order to clearly understand how the changes in its photophysical and/or electrochemical properties can actually influence the photocatalytic activity of a certain catalyst. Interestingly, although a derivatization approach was recently attempted mainly directed to the formation of supramolecular sensitizer-catalyst assemblies,[10] detailed studies are currently absent in the literature concerning the relationship between the structure of the ruthenium chromophore and the resulting photocatalytic activity in a homogeneous donor/sensitizer/catalyst three-component system.

Herein we report on photocatalytic hydrogen evolution studies involving a series of ruthenium polypyridine complexes as the photosensitizers (Chart 1). In particular, the choice of the ruthenium complexes (**Ru1-4**) is such that the optical properties are appreciably similar throughout the series whereas the introduction of different functional groups mainly affects their electrochemical behavior. A cobaloxime complex (**CoDMG**) has been taken as the catalyst of reference, since its electrochemical properties as well as its catalytic behaviour (e.g., HER mechanism, degradation issues, etc.) are well established.[11] Finally, ascorbic acid (**AscH**) has been used as the sacrificial donor in order to provide acidic conditions which the hydrogen evolving reaction may benefit from. Detailed photophysical studies have been also undertaken in order to define the operating photocatalytic mechanism and to get a deeper understanding on the relationship between the structure and properties of the sensitizer and the actual hydrogen evolving activity of the related three-component system.

Chart 1. Molecular structures of the compounds used in this work.

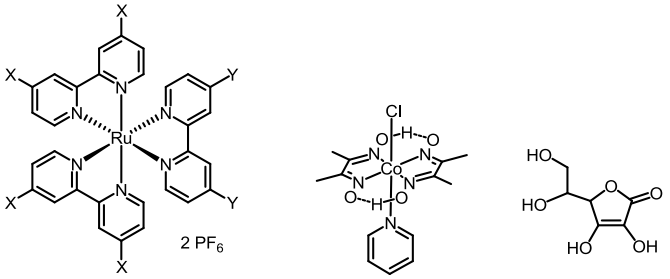

Ru1 X = Y = H
Ru2 X = H Y = Me
Ru3 X = Y = Me
Ru4 X = Y = *t*Bu

CoDMG **AscH**

Results and Discussions

Optical and electrochemical properties.

The optical and electrochemical properties of the whole class of ruthenium complexes **Ru1-4** were studied in a 50/50 acetonitrile/water mixture as the target solvent for the photocatalytic hydrogen evolution experiments.[7,11c] All spectroscopic and electrochemical data are summarized in Table 1, in which the electrochemical data of the **CoDMG** catalyst and the **AscH** sacrificial donor are also indicated. As it can be promptly observed, the optical properties of the ruthenium complexes are comparable along the series with the absorption and emission maxima varying within a very narrow wavelength window, consistent also with the comparable differences between the oxidation and reduction potentials. This observation is of particular importance in view of the hydrogen evolution experiments (see Experimental Section below): the irradiation is indeed performed over the whole visible spectrum (400-800 nm) and thus a straightforward comparison of the photocatalytic activity is

Table 1. Summary of the optical and electrochemical data of complexes **Ru1-4** together with the electrochemical data of **CoDMG** and **AscH** in a 50/50 acetonitrile/water mixture.

Compound	Absorption λ_{max} (nm)	Emission λ_{max} (nm)	E^{0-0} (eV) [a]	E_{ox} (V vs SCE) [b]	$E_{red}^{(1)}$ (V vs SCE) [b]	$E_{red}^{(2)}$ (V vs SCE) [b]
Ru1	452	612	2.25	+1.17	−1.41	
Ru2	455	618	2.22	+1.10	−1.44 [d]	−1.63 [d]
Ru3	459	620	2.21	+1.00	−1.54	
Ru4	459	618	2.23	+1.04	−1.42	
CoDMG					−0.54 [e,g]	−1.00
AscH [c]				+0.45 [f,g]		

[a.] excited-state energy estimated from the onset (5% relative intensity) of the room-temperature emission spectrum (according to ref. 12); [b.] obtained by cyclic voltammetry (CV) at 298 K, scan rate 100 mV/s, 0.1 M $LiClO_4$ solution in 50/50 acetonitrile/water; [c.] buffered at pH 5 upon addition of NaOH (few droplets from a 5 M stock solution in water); [d.] obtained by differential pulse voltammetry (DPV), pulse width of ΔE = 50 mV; [e.] cathodic peak potential; [f.] anodic peak potential; [g.] irreversible process.

meaningful only in the case of a similar absorption profile. On the other hand, the presence of different functional groups in the 4,4' position of the bipyridine ligand has a remarkable effect on the electrochemical properties, resulting in both lower oxidation and reduction potentials upon introduction of electron-donating groups.

Photochemistry of the sensitizer/donor two-component system.

The emission of all the ruthenium complexes **Ru1-4** in the 50/50 acetonitrile/water mixture (Figure S1a, S2a, S3a, and S4a of the ESI) is progressively quenched upon addition of different amounts of **AscH**, buffered at pH 5 with NaOH. The quenching process is mostly dynamic, as it can be observed from the comparison of the time-resolved emission profiles at different **AscH** content (Figure S1b, S2b, S3b, and S4b). Only a small difference in the prompt emission signal (< 5-10%) can be observed and reasonably attributed to a static quenching process, most likely as a result of ground state electrostatic interactions between the positively charged sensitizers and the negatively charged sacrificial donor (at pH 5 ascorbic acid, pK_a = 4.1, is indeed largely dissociated and thus it is mainly present in solution as ascorbate anion). As to the mechanism, reductive excited state quenching is the only possibility, involving reduction of the excited sensitizer and oxidation of the ascorbic acid donor (eq 1-7). As a bimolecular process, the photoreaction can be split into several contributions: the photoexcitation (eq 1), the diffusion step (eq 2), the electron transfer within the encounter complex (eq 3), the escape from the solvent cage (eq 4), and eventually the charge recombination (eq 5-7). Being a bimolecular process as well, the latter can be divided into its various contributions, namely the diffusion (eq 5), the reaction (eq 6), and the product separation (eq 7).

$$Ru + h\nu \rightarrow {}^1*Ru \rightarrow {}^3*Ru \quad (1)$$
$$^3*Ru + \mathbf{AscH} \rightarrow [^3*Ru \mid \mathbf{AscH}] \quad (2)$$
$$[^3*Ru \mid \mathbf{AscH}] \rightarrow [Ru^- \mid \mathbf{AscH}^+] \quad (3)$$
$$[Ru^- \mid \mathbf{AscH}^+] \rightarrow Ru^- + \mathbf{AscH}^+ \quad (4)$$
$$Ru^- + \mathbf{AscH}^+ \rightarrow [Ru^- \mid \mathbf{AscH}^+] \quad (5)$$
$$[Ru^- \mid \mathbf{AscH}^+] \rightarrow [Ru \mid \mathbf{AscH}] \quad (6)$$
$$[Ru \mid \mathbf{AscH}] \rightarrow Ru + \mathbf{AscH} \quad (7)$$

Plot of I_0/I and τ_0/τ in all cases show some deviation with respect to the linear Stern-Volmer behavior (Figure 1). In fact the addition of ascorbate, beside improving the quenching efficiency, simultaneously brings about an increase of the ionic strength of the solution. Being the reactants ionic species, this latter effect negatively influences the diffusion step of the bimolecular electron transfer process (eq 2),[13] resulting in an apparent, progressive loss of quenching efficiency upon increasing the quencher concentration. This notwithstanding, an approximation of the bimolecular rate constant for the excited state quenching by **AscH** can be obtained at low quencher concentrations (in the present case at [**AscH**] ≤ 0.02 M).[14] Under these conditions smaller variations of the ionic strength of the solution are indeed expected, resulting in appreciably linear plots of I_0/I (or τ_0/τ) vs. [**AscH**], thus amenable to a classical Stern-Volmer treatment. These estimates yields bimolecular rate constants of $k = 1.6 \times 10^8$ $M^{-1}s^{-1}$ for **Ru1**, $k = 1.1 \times 10^8$ $M^{-1}s^{-1}$ for **Ru2**, $k = 2.8 \times 10^7$ $M^{-1}s^{-1}$ for **Ru3**, and $k = 3.7 \times 10^6$ $M^{-1}s^{-1}$ for **Ru4**. Interestingly, in the case of complexes **Ru1-3** the bimolecular rate constants are appreciably dependent on the oxidizing ability of the excited triplet manifold of the sensitizers (E = +0.84 V vs. SCE for **Ru1**, E = +0.78 V vs. SCE for **Ru2**, and E = +0.67 V vs. SCE for **Ru3**) and thus with the driving forces of the electron transfer process (ΔG = −0.39 eV for **Ru1**, ΔG = −0.33 eV for **Ru2**, and ΔG = −0.22 eV for **Ru3**, neglecting electrostatic work terms), resulting in faster rates for more exergonic processes. This evidence thus indicates that the reductive electron transfer from the **AscH** sacrificial donor to the excited ruthenium sensitizer occurs in the Marcus normal region. Notably, in spite of the larger driving force with respect to both **Ru2** and **Ru3**, reductive quenching of **Ru4** by **AscH** (ΔG = −0.36 eV) is slower by more than one order of magnitude. This can be reasonably attributed to the presence of the bulky *tert*-butyl groups which significantly reduces the electronic coupling between the donor and acceptor orbitals within the encounter complex (eq 3).[15]

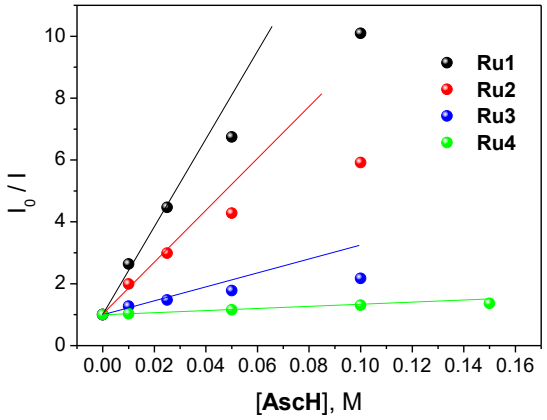

Figure 1. Stern-Volmer plots of the excited state quenching of **Ru1-4** by the ascorbate sacrificial donor (**AscH**, buffer at pH 5) in nitrogen-purged 50/50 acetonitrile/water solution.

The excited state reductive quenching by the ascorbate donor is expected to yield the reduced species of the sensitizer. Its generation and evolution in time can be conveniently monitored by transient absorption spectroscopy, as the reduced sensitizers display a featuring absorption at around 500 nm.[16] At a fixed **AscH** concentration of 0.1 M (buffered at pH 5), the overall yield of reduced sensitizer obtained upon 355-nm excitation of 50/50 acetonitrile/water solutions containing 0.1 mM **Ru1-4** follows, as expected, a direct correlation with the bimolecular rate constants of the excited state quenching, resulting in larger yields in the order **Ru1** > **Ru2** > **Ru3** > **Ru4** (Figure 2 and Table 2). From the comparison of the theoretical maximum yield of charge separated products, calculated from the quenching efficiency

Table 2. Bimolecular rate constants and quantum yields of the reductive electron transfer quenching process involving the ruthenium complexes **Ru1-4** and **AscH** in nitrogen-purged 50/50 acetonitrile/water.

Compound	k_Q (10^7 $M^{-1}s^{-1}$) [a]	η_Q [b]	Φ^{Ru^-} [c]	Φ_{ce}	k_{CR} (10^9 $M^{-1}s^{-1}$) [d]
Ru1	16	0.90	0.88	0.98	2.7
Ru2	11	0.83	0.79	0.95	2.7
Ru3	2.8	0.54	0.42	0.78	4.7
Ru4	0.37	0.24	0.18	0.75	3.8

[a.] Obtained from a Stern-Volmer treatment at [**AscH**] < 0.05 M; [b.] [**AscH**] = 0.1 M; [c.] calculated according to footnote ‡; [d.] obtained according to second-order kinetic law from the decay of the reduced sensitizer transient absorption signal (Figure S5, S6, S7, and S8).

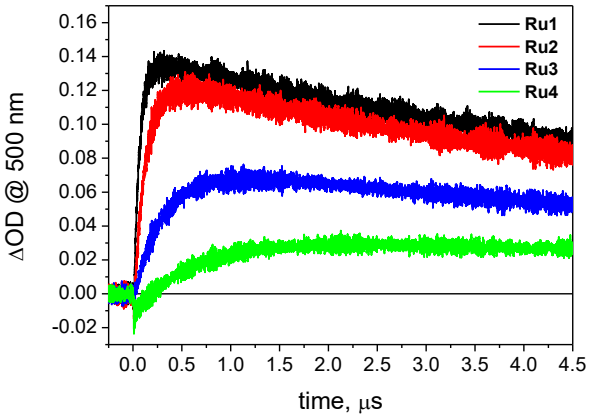

Figure 2. Kinetic traces of the reduced sensitizer formation followed at 500 nm by laser flash photolysis (excitation at 355 nm, FWHM = 6-8 ns) on nitrogen-purged 50/50 acetonitrile/water solution containing 0.1 M **AscH** (buffered at pH 5) and 0.1 mM **Ru1** (black trace), 0.1 mM **Ru2** (blue trace), 0.1 mM **Ru3** (green trace), and 0.1 mM **Ru4** (orange trace).

at 0.1 M **AscH**, and the actual experimental data, as possibly estimated from the kinetic traces of Figure 2,‡ cage escape yields (eq 4) close to unity are determined for complexes **Ru1** and **Ru2**, consistent with the values obtained in purely aqueous solutions for **Ru1**,[18] whereas for complexes **Ru3** and **Ru4** slightly lower apparent values (0.78 and 0.75, respectively) can be obtained from the maxima in the transient changes of Figure 2.§ All the relevant photophysical data are summarized in Table 2.

In the absence of any electron acceptor (e.g., a catalyst) the charge separated species, namely the reduced sensitizer and the oxidized ascorbate donor, undergoes bimolecular charge recombination (eq 5-7) in a time scale of hundreds μs.§§ This process can be monitored from the decay of the transient signal of the reduced sensitizers at 500 nm in a time window of ca 200 μs (Figure S5a, S6a, S7a, and S8a for **Ru1**, **Ru2**, **Ru3**, and **Ru4**, respectively) and the related kinetic traces can be treated according to a second-order kinetic law (Figure S5b, S6b, S7b, and S8b). As a result, considering the molar extinction coefficient of the reduced ruthenium species[16] and the "actual" optical path,¶ bimolecular rate constants of k = 2.7 × 10^9 $M^{-1}s^{-1}$ for both **Ru1** and **Ru2**, k = 4.7 × 10^9 $M^{-1}s^{-1}$ for **Ru3**, and k = 3.8 × 10^9 $M^{-1}s^{-1}$ for **Ru4** can be obtained for the charge recombination process (Table 2). It should be noticed that the dependence of the charge recombination rates on driving force (ΔG = −1.86 eV for **Ru1**, ΔG = −1.89 eV for **Ru2**, ΔG = −1.99 eV for **Ru3**, and ΔG = −1.87 eV for **Ru4**) is, if any, much weaker than for charge separation. Along with their high absolute values, close to the diffusion-limited regime, the weak driving force dependence is consistent with the charge recombination processes lying close to the Marcus activationless regime.

In the forward quenching reaction, the sharp drop in rate observed for **Ru4** relative to the **Ru1-3** series was attributed to the steric hindrance of the *tert*-butyl groups and its effect on the donor-acceptor electronic coupling.[15] Interestingly, no such drop is experimentally obtained for charge recombination (Table 2). This difference may be related to the different nature of the orbitals involved in the two types of processes. In fact, for the forward electron transfer the donor-acceptor interactions involved are at the HOMO-HOMO level (i.e., between the HOMO of the **AscH** donor, whose electron density mainly resides on the hydroxo and carbonyl groups of the furan ring,[21] and the HOMO of the ruthenium complex which is a metal-centered *d* orbital). In the backward reaction, on the other hand, HOMO-LUMO interactions are implicated (i.e., between the same HOMO for **AscH** and a ligand-centred π* LUMO for the ruthenium sensitizers). This implies that different distances and orbital overlaps are involved in the two electron transfer reactions within the encounter complex (eq 3 and 6). Hence, with respect to the long-distance, weak-interaction forward process, the steric effect of the 4,4' substituents in the bpy ligand is likely to be substantially attenuated for the short-distance, strong-interaction charge recombination reaction.

Photochemistry of the sensitizer/catalyst two-component system.

When different amounts of **CoDMG** catalyst are added to a solution of **Ru1-4** in a 50/50 acetonitrile/water mixture, quenching of the emission is observed. This quenching process is entirely dynamic, as expected on the basis of the neutral character of the **CoDMG** complex, and good Stern-Volmer plots are indeed obtained for all the **Ru1-4** complexes (Figure S9, S10, S11, and S12 of the ESI), yielding diffusion-controlled (at least for **Ru1**, **Ru2**, and **Ru3**) bimolecular rate constants of k = 9.6 × 10^9 $M^{-1}s^{-1}$ for **Ru1**, k = 9.4 × 10^9 $M^{-1}s^{-1}$ for **Ru2**, k = 1.1 × 10^{10} $M^{-1}s^{-1}$ for **Ru3**, and k = 5.9 × 10^9 $M^{-1}s^{-1}$ for **Ru4** (Table 3). As to the quenching mechanism two possible pathways are in principle thermodynamically allowed: (i) oxidative photoinduced electron transfer involving oxidation of the ruthenium sensitizer and reduction of the **CoDMG** catalyst (eq

8-11) to a cobalt(II) species and (ii) electronic energy transfer to the cobalt center (eq 8,12-14) which has low-lying *d-d* states potentially accessible from the ruthenium MLCT excited triplet manifold.[22]

^{3}*Ru + **CoDMG** → [^{3}*Ru | **CoDMG**] (8)
[^{3}*Ru | **CoDMG**] → [Ru$^+$ | **CoDMG**$^-$] (9)
[Ru$^+$ | **CoDMG**$^-$] → Ru$^+$ + **CoDMG**$^-$ (10)
Ru$^+$ + **CoDMG**$^-$ → Ru + **CoDMG** (11)
[^{3}*Ru | **CoDMG**] → [Ru | ***CoDMG**] (12)
[Ru | ***CoDMG**] → Ru + ***CoDMG** (13)
Ru + ***CoDMG** → Ru + **CoDMG** (14)

To get experimental insight into the quenching mechanism, transient absorption spectroscopy studies have been applied. The results are reported in Figure 3 for **Ru1**, and in Figure S13, S14, and S15 for **Ru2**, **Ru3**, and **Ru4**, respectively. Upon excitation at 355 nm of a 50/50 acetonitrile/water solution containing 0.1 mM **Ru1-4** complex and 0.25 mM **CoDMG** (in these conditions the efficiency of the excited state quenching by the cobaloxime catalyst is ca 70%) the transient spectrum which is immediately observed after the laser pulse (time-delay of t = 10 ns), featuring the MLCT bleach at ca 450 nm and the positive absorption of the reduced bpy ligand at ca 380 nm, corresponds to the triplet MLCT excited state of the ruthenium sensitizer. In all cases this transient spectrum is observed to decay monotonically to the baseline within a μs without formation and accumulation of additionally transient signatures.

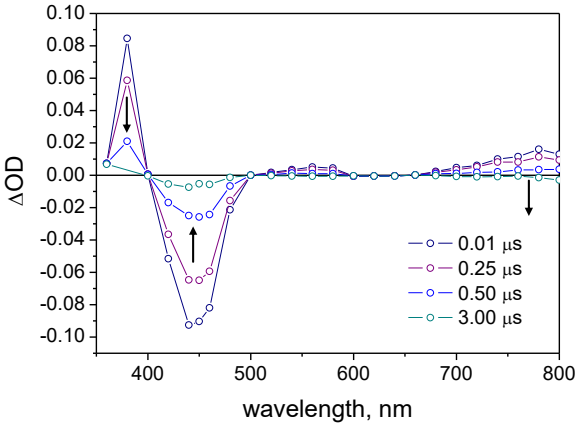

Figure 3. Transient absorption spectra at different time delays obtained by laser flash photolysis (excitation at 355 nm, FWHM = 6-8 ns) on a 50/50 acetonitrile/water solution containing 0.1 mM **Ru1** and 0.25 mM **CoDMG**.

These spectral changes are both compatible with an oxidative photoinduced electron transfer pathway (hypothesis i, eq 8-11) but featuring negligible cage escape yields, and with an energy transfer mechanism (hypothesis ii, eq 8,12-14), since excited states of 3d metal complexes are known to be exceedingly short-lived.[23] As a result, in both cases any sizeable accumulation of charge separated products is prevented and a simple decay of the excited triplet MLCT manifold to the ground state is expected. Regardless of the mechanism, however, excited state quenching by the cobaloxime catalyst **CoDMG** proves to be ineffective in the photocatalytic hydrogen evolution studies within a donor/sensitizer/catalyst three-component system.

Table 3. Bimolecular rate constants of triplet excited state quenching by **CoDMG** and electron transfer from the reduced sensitizer to **CoDMG**$^-$.

Compound	k_{3*Ru} (10^9 $M^{-1}s^{-1}$) [a]	k_{Ru^-} (10^9 $M^{-1}s^{-1}$) [b]
Ru1	9.6	4.8
Ru2	9.4	6.9
Ru3	11	5.4
Ru4	5.9	3.0

[a.] Obtained from Stern-Volmer analyses (Figure S9, S10, S11, and S12); [b.] obtained from the transient decays of the reduced sensitizer species at 500 nm (Figure 4, S18, S19, and S20).

Photochemistry of the donor/sensitizer/catalyst three-component system.

In the three-component system, the concentrations of the **CoDMG** catalyst and the ascorbate donor play a crucial role in determining the fate of the excited ruthenium sensitizer. In the hydrogen evolution experiments (*vide infra*) the concentration of the **CoDMG** catalyst was fixed at 0.1 mM, as this type of catalyst was usually shown to be active in photochemical cycles at concentration ≥0.1 mM,[11] whereas the concentration of the **AscH** sacrificial donor was kept between 0.01-0.1 M, depending on the type of experiment (see below). Under the photocatalytic conditions, the pseudo-first order rates are such that the reductive quenching by the ascorbate sacrificial donor is much faster than the quenching by the **CoDMG** catalyst. This implies that under the photocatalytic conditions reductive quenching of the triplet excited state of the sensitizer by the ascorbate donor is the dominating photochemical pathway and thus the hydrogen evolving mechanism is *reductive* in nature (see above, Scheme 1b). In summary, upon light excitation the excited triplet state of the photosensitizer is subjected to a reductive quenching by the ascorbate sacrificial donor (eq 1-4) and, in competition with charge recombination (eq 5-7), the reduced sensitizer undergoes electron transfer to the catalyst thus starting the charge accumulation within the catalytic site to trigger the hydrogen evolving activity.

Before evaluating in detail the kinetics of this latter electron transfer step, it is important to point out the actual nature of the **CoDMG** species within the donor/sensitizer/catalyst three-component system examined. The following experimental data indeed aim at clarifying this key issue. When a **CoDMG** solution (50/50 acetonitrile/water, 0.1 M $LiClO_4$) is probed by cyclic voltammetry in the presence of 0.1 M **AscH** (buffered at pH 5 with NaOH), the disappearance of the first cathodic process attributable to the Co(III)/Co(II) reduction is observed (Figure S16). Not only, after few minutes aging of a **CoDMG** 50/50 acetonitrile/water solution in the presence of 0.1 M **AscH** (buffered at pH 5) the absorption spectrum exhibits the development of a new band, which is centered at ca 450 nm and is typical of cobalt(II) cobaloxime-type complexes (Figure S17).[24] Both results confirm that a thermal reduction of **CoDMG** to **CoDMG**$^-$ is induced by the ascorbate.‖ Importantly,

this process should be accompanied by the detachment of the axial chloride ligand,[25] leaving a 5-coordinated cobalt(II) center with a free axial position available for the formation of catalytically relevant intermediates. In summary, in the donor/sensitizer/catalyst three-component system the **CoDMG** is always present as a cobalt(II) species and thus the electron transfer process from the reduced **Ru1-4** sensitizer (eq 15-17) does imply the generation of a formal Co(I) moiety.

$$Ru^{-} + \mathbf{CoDMG}^{-} \rightarrow [Ru^{-} \mid \mathbf{CoDMG}^{-}] \quad (15)$$
$$[Ru^{-} \mid \mathbf{CoDMG}^{-}] \rightarrow [Ru \mid \mathbf{CoDMG}^{2-}] \quad (16)$$
$$[Ru \mid \mathbf{CoDMG}^{2-}] \rightarrow Ru + \mathbf{CoDMG}^{2-} \quad (17)$$

According to these considerations, it is possible to experimentally monitor the electron transfer process from the photogenerated reduced sensitizer to the **CoDMG**$^{-}$ catalyst through laser flash photolysis experiments upon excitation of 50/50 acetonitrile/water solutions containing the ruthenium sensitizer (0.1 mM) and 0.1 M **AscH** (buffered at pH 5) and following the fate of the 500-nm transient signal upon addition of different amounts of **CoDMG** catalyst (see, e.g., Figure 4a for **Ru1**). The transient absorption signal of the reduced sensitizer at 500 nm is indeed observed to decay to the baseline with kinetics which are dependent on catalyst concentration. This means that the photogenerated reduced sensitizer undergoes bimolecular electron transfer to the **CoDMG**$^{-}$ catalyst (eq 15-17). Under pseudo-first order kinetic conditions the traces can be fitted with single-exponential functions and the so obtained pseudo-first order rates can be divided by the concentration of the catalyst to get the bimolecular rate constant. These estimates yield values of k = 4.8×10^{9} $M^{-1}s^{-1}$ for **Ru1**, k = 6.9×10^{9} $M^{-1}s^{-1}$ for **Ru2**, k = 5.4×10^{9} $M^{-1}s^{-1}$ for **Ru3**, and k = 3.0×10^{9} $M^{-1}s^{-1}$ for **Ru4** (Figure 4b, S18, S19, and S20 for **Ru1**, **Ru2**, **Ru3**, and **Ru4**, respectively, Table 3). These fast rates are consistent with the involvement of a Co(II)/Co(I) reduction process rather than a Co(III)/Co(II) one which should be, on the other hand, intrinsically slow, being accompanied by a large reorganization energy.[11d,e,22a] As already noticed for the reactions with the oxidized ascorbate (see above, Table 2), these fast rates for the electron transfer from the reduced sensitizers to the catalyst are relatively constant throughout the series, with weak, if any, dependence on the driving force. A hint of steric hindrance effect[15] may be, however, considered for the relatively slower rate of the **Ru4** system.

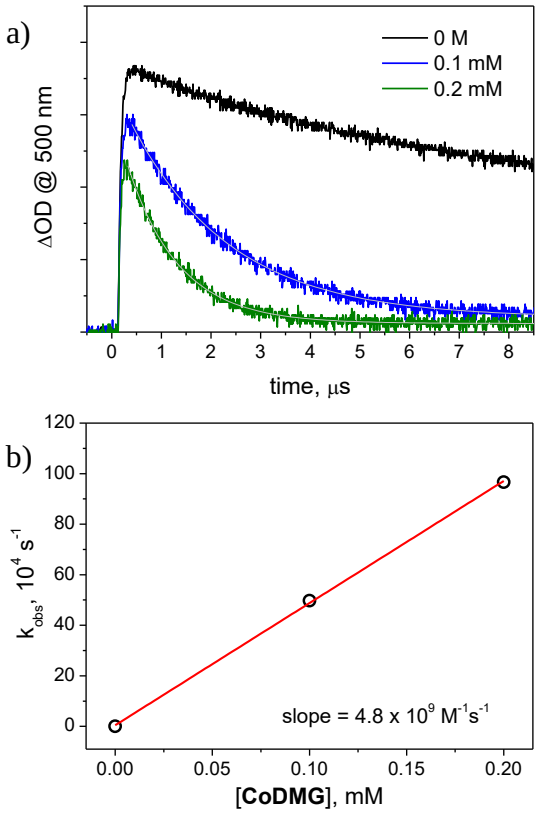

Figure 4. (a) Kinetic traces at 500 nm (with related exponential fitting) obtained by laser flash photolysis (excitation at 355 nm, FWHM = 6-8 ns) on a 50/50 acetonitrile/water solution containing 0.1 mM **Ru1**, 0.1 M **AscH** (buffered at pH 5), and 0-0.2 mM **CoDMG**. (b) Plot of the pseudo-first order rate vs. the **CoDMG** concentration for the estimation of the bimolecular rate constant.

It must be also remarked that from the spectroscopic viewpoint the reduction of **CoDMG**$^{-}$ to **CoDMG**$^{2-}$ (eq 15-17) should be characterized by the formation of a positive absorption in the 500-700 nm region.[24] However, the fingerprint of the reduced sensitizer (i.e., the absorption centered at ca 500 nm, see, e.g., for **Ru1**, Figure S21) decays monotonically to the baseline without formation of additional transient signatures, i.e., those expected for the appearance of a cobalt(I) species (**CoDMG**$^{2-}$). The failure to observe such spectral features can be attributed to the fact that the electron transfer from the reduced sensitizer to the cobalt center takes place together with a protonation step (eq 18) as a concerted proton-coupled electron-transfer (PCET) process (eq 19) to give a dioxime hydrido cobalt(III) moiety (H-**CoDMG**). This is also consistent with the observation that cobalt(III)-hydride species display negligible absorption above 500 nm.[26]

$$\mathbf{CoDMG}^{2-} + H^{+} \rightarrow \text{H-}\mathbf{CoDMG} \quad (18)$$
$$Ru^{-} + \mathbf{CoDMG}^{-} + H^{+} \rightarrow Ru + \text{H-}\mathbf{CoDMG} \quad (19)$$

Photocatalytic hydrogen evolution experiments.

Once the cobalt(III)-hydride catalytic intermediate is formed through the sequence of photoinduced and thermal electron transfer processes described above, additional reduction/protonation steps (eq 20,21) are then expected to enable hydrogen evolution.[11d,e]

$$Ru^{-} + \text{H-}\mathbf{CoDMG} \rightarrow Ru + \text{H-}\mathbf{CoDMG}^{-} \quad (20)$$
$$\text{H-}\mathbf{CoDMG}^{-} + H^{+} \rightarrow \mathbf{CoDMG}^{-} + H_2 \quad (21)$$

When hydrogen has been released (eq 21) the cobaloxime catalyst is recovered to its original form, ready to enter a new photo-activated catalytic cycle.

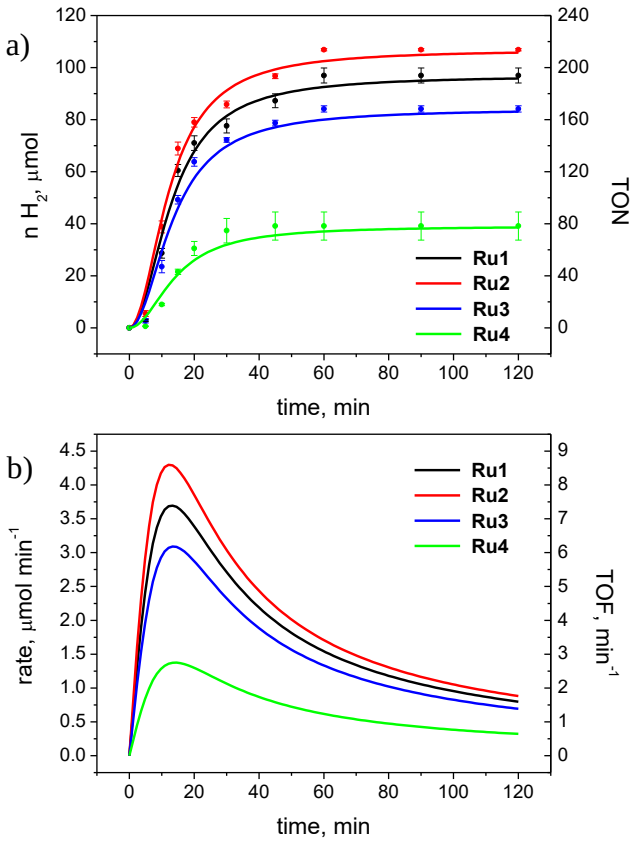

Figure 5. Photocatalytic hydrogen evolution experiments (50/50 acetonitrile/water, 0.5 mM **Ru1-4**, 0.1 mM **CoDMG**, 0.1 M **AscH** buffered at pH 5): (a) hydrogen evolving kinetics and (b) rates.

The actual ability of the three-component systems to power light-assisted hydrogen evolution was thus assessed by continuous visible irradiation, at first, using standard conditions,[5a,d,f,6-8] namely 50/50 acetonitrile/water solutions containing 0.5 mM **Ru1-4** sensitizer, 0.1 mM **CoDMG** catalyst, and 0.1 M **AscH** buffered at pH 5 with small additions from a 5 M NaOH stock solution (see Experimental Section for additional details). Related kinetic traces (averages of two different experiments) are reported in Figure 5 and relevant photocatalytic data are reported in Figure 6.

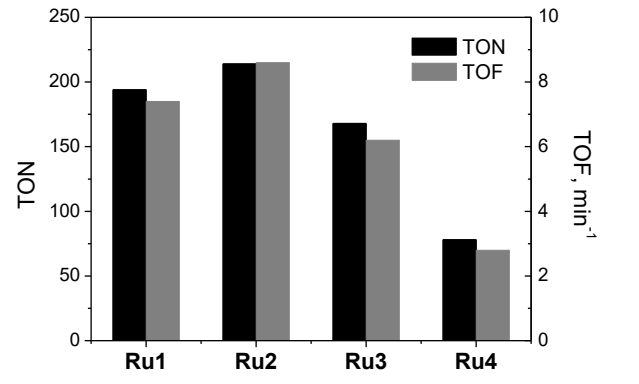

Figure 6. Relevant photocatalytic data from the hydrogen evolution kinetics of Figure 5.

In all three cases, upon light irradiation hydrogen evolution starts after a small induction period (few minutes) with rates between 1.4 and 4.3 µmol min^{-1} depending on the sensitizer (corresponding to maximum turnover frequencies between 2.8 and 8.6 min^{-1}) and levels off after ca 1-2 hours when maximum turnover numbers between 78 and 214 can be estimated (Figure 6). More interestingly, the kinetic performances and thus the photocatalytic data are appreciably dependent upon the sensitizer employed resulting in both larger TONs and TOFs in the order **Ru2** > **Ru1** > **Ru3** > **Ru4**.

On a qualitative basis, the faster initial hydrogen production rates observed (larger maximum TOFs), corresponding to larger quantum yields for hydrogen evolution (the initial rates are indeed obtained in the linear part of the kinetic traces), can be correlated with the more favorable kinetics and thus the higher efficiencies of the electron transfer processes (photoinduced and thermal ones) involved within the photocatalytic reaction scheme, namely the photogeneration of the reduced sensitizer (eq 1-4) and the activation of the catalyst (eq 15-17). Faster rates for the reductive quenching of the sensitizer by **AscH** are indeed measured for complexes **Ru1** and **Ru2** with respect to **Ru3** and **Ru4** (see Table 2), whereas the fastest electron transfer to the catalyst is detected for complex **Ru2** (see Table 3). This may actually explain why sensitizer **Ru2** outperforms the other complexes under the standard conditions employed. As far as the maximum TONs are concerned, rather similar values are observed for complexes **Ru1** and **Ru2** (194 and 214, respectively, Figure 6), whereas a slight decrease is seen for **Ru3** (TON = 168) and an appreciably lower value is measured for complex **Ru4** (TON = 78). The reason for this difference lies on the fact that, while for complexes **Ru1** and **Ru2** the turnover limiting reaction is mainly the degradation of the cobaloxime catalyst, which is known to occur via hydrogenation of the dimethylglioximate ligands,[11] in the case of complex **Ru4** and to a lesser extent of **Ru3** a considerable decomposition of the sensitizer is also noticed (see the comparison of the absorption spectra before/after photolysis in Figure S22).# A comparison of the relative rates of reductive quenching by **AscH** and electron transfer to the **CoDMG** catalyst within the **Ru1-4** series is still informative to account for these observations. In fact, the degradation of a ruthenium polypyridine sensitizer in photochemical hydrogen evolution experiments is usually attributed to (1) photosubstitution reactions by the solvent or the ascorbate donor occurring via thermal population of the closely lying ^{3}MC *d-d* states in competition with the reductive quenching by the sacrificial donor[5c,6] or (2) degradation of the reduced photosensitizer in competition with electron transfer to the catalyst.[8,27] The fastest reductive quenching rates observed for **Ru1** and **Ru2** when compared to those of **Ru3** and particularly **Ru4** are thus favorable to minimize the detrimental photosubstitution pathway (hypothesis 1), while the highest electron transfer rates for catalyst reduction

measured for **Ru1**, **Ru2**, and **Ru3** are advantageous for decreasing the probability of sensitizer degradation via its reduced form (hypothesis 2).

Overall these results strongly suggest that complexes **Ru1** and **Ru2** are better photosensitizers for photochemical hydrogen evolution experiments than complexes **Ru3** and **Ru4**. At this point, to get a more quantitative comparison between the hydrogen evolving ability of the donor/sensitizer/catalyst three-component system taking advantage of either **Ru1** or **Ru2** as the light-harvesting chromophore the photocatalytic activity of both the **AscH**/**Ru1**/**CoDMG** and the **AscH**/**Ru2**/**CoDMG** systems was studied upon continuous visible irradiation of 50/50 acetonitrile/water solutions containing 0.5 mM **Ru1**/**Ru2** sensitizer, 0.1 mM **CoDMG** catalyst, but employing a concentration of **AscH** (buffered at pH 5) such that the efficiency of the triplet excited state quenching by the donor was identical (i.e., ca 70%) for both **Ru1** and **Ru2**. The results are shown in Figure 7 (where kinetic traces are averages of two different experiments).

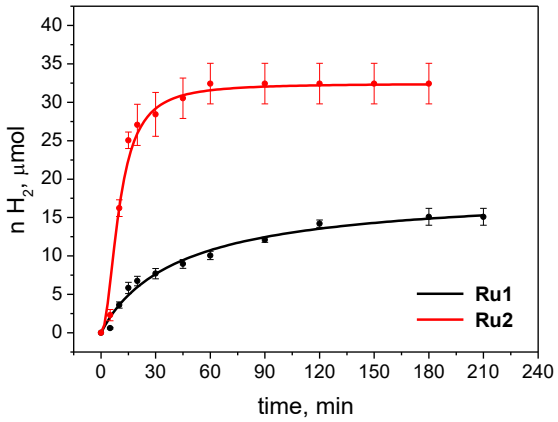

Figure 7. Photocatalytic hydrogen evolution experiments (50/50 acetonitrile/water, 0.5 mM **Ru1**/**Ru2**, 0.1 mM **CoDMG**) at identical excited state quenching yield (ca 70%) by the **AscH** (12 mM and 27 mM for **Ru1** and **Ru2**, respectively, both buffered at pH 5).

It is worth pointing out that a straightforward comparison of the hydrogen evolving activity in these latter conditions is only meaningful in terms of initial hydrogen production rates (or maximum TOFs), which are intimately connected to the quantum yield of the photoreaction (i.e., when the hydrogen production is appreciably linear in time), rather than in terms of TONs. Indeed the appreciably low concentration of **AscH** in the photolyzed solutions (ca 4 times lower for **Ru2** and ca 10 times lower for **Ru1** with respect to the standard conditions, Figure 5) is such that the buffering capacity of the irradiated mixture is intrinsically weak (a pH of ca 8 and of ca 7 is measured after irradiation of the **AscH**/**Ru1**/**CoDMG** and the **AscH**/**Ru2**/**CoDMG** systems, respectively, in spite of the smaller amounts of hydrogen produced with respect to the standard conditions, see above, Figure 5). As a consequence, these evidences do give important uncertainties in the determination of the turnover limiting factors and their correlation with the relevant kinetic data.

Accordingly, considerably faster hydrogen production rates are observed for the three-component system involving complex **Ru2** as the light-harvesting sensitizer (initial rate of 1.6 μmol min^{-1} corresponding to a maximum TOF of 3.2 min^{-1}) with respect to the one with the **Ru1** chromophore (initial rate of 0.5 μmol min^{-1} corresponding to a maximum TOF of 1.0 min^{-1}), well correlating with the electron transfer rate from the reduced sensitizer to the cobaloxime catalyst being faster for **Ru2** than for **Ru1** (see Table 3). Since two electron transfer processes are required for the activation of the **CoDMG** catalyst and a comparable difference in terms of kinetics can be in principle envisioned also for the second electron transfer (eq 20), even small differences in one-electron transfer rates are expected to considerably account in fostering catalysis, thus explaining the substantial enhancement in terms of hydrogen evolving performance obtained in the **AscH**/**Ru2**/**CoDMG** system. These results clearly establish that complex **Ru2** is a suitable chromophore, even superior to the commonly used **Ru1**, to be exploited in light activated experiments for hydrogen evolution, combining the right balance among excited state redox properties, reducing ability of the $\mathbf{Ru2}^{-}$ species, and steric hindrance.

Conclusions

Homogeneous systems for photocatalytic hydrogen evolution have been described which consist of a ruthenium polypyridine sensitizer (**Ru1-4**), a cobaloxime catalyst (**CoDMG**), and ascorbic acid (**AscH**) as the sacrificial electron donor. Different groups have been added in the 4,4'-position of the bipyridine ligands in order to alter the redox properties of the sensitizer as well as its bulkiness without affecting their optical properties. Detailed photochemical studies of the sensitizer/donor, sensitizer/catalyst two-component systems and of the donor/sensitizer/catalyst three-component system have been performed in order to obtain information on the operating photocatalytic mechanism, to characterize the kinetics of the relevant electron transfer processes involved in the hydrogen evolving reaction mechanism, and in particular to rationalize the observed differences in photocatalytic behavior. It turns out that a good balance among i) excited state redox properties of the sensitizer, affecting the reductive quenching rate by the sacrificial donor, ii) reducing ability of the photogenerated reduced species of the chromophore, determining the rate of electron transfer to the catalyst, and iii) steric hindrance of the complex, affecting the electronic coupling within the encounter complex in both electron transfer processes, is the winning strategy to identify a successful sensitizer. Accordingly, this is what makes complex **Ru2** a suitable sensitizer, even superior to the standard $Ru(bpy)_3^{2+}$ chromophore, to be exploited for the characterization of new hydrogen evolving catalysts.

Experimental Section

Materials.

Spectroscopic grade acetonitrile was purchased from Sigma-Aldrich and used for both the spectroscopic and photolysis experiments. Milli-Q Ultrapure water was used. All other reagents and chemicals were purchased from Sigma-Aldrich and used as received.

Synthesis.

The preparation of **Ru1** has been performed as a simple precipitation procedure starting from commercially available reagents. The synthesis of complexes **Ru2**, **Ru3**, and **Ru4** have been adapted from reported literature procedures,[28-30] whereas the synthesis of the cobaloxime complex has been performed according to Schrauzer.[31]

Tris(2,2'-bipyridine)ruthenium(II) dihexafluorophosphate (**Ru1**). Commercially available (Sigma-Aldrich) tris(2,2'-bipyridine) ruthenium(II) dichloride hexahydrate (350 mg, 0.46 mmol) was dissolved in 15 mL of water. Few droplets of hexafluorophosphoric acid were added. The precipitate formed was then filtered on a Büchner funnel and washed with cold water, ethanol, and ether. The red/orange solid was recovered and dried in an oven at 50°C for 5 hours.

(4,4'-dimethyl-2,2'-bipyridine)bis(2,2'-bipyridine)ruthenium(II)dihexafluorophosphate (**Ru2**). 1 equivalent of bis(2,2'-bipyridine) dichloro ruthenium(II) (200 mg, 0.4 mmol) was dissolved in 20 mL DMF, 1 equivalent of 4,4'-dimethyl-2,2'-bipyridine (76 mg, 0.4 mmol) was then added and the mixture was heated under reflux for several hours under continuous stirring. The reaction was followed by thin-layer chromatography (silica, 9/1 ethyl acetate/dichloromethane) and by UV-Vis absorption (monitoring the formation of the MLCT absorption at ca. 450 nm). After completion, the mixture was cooled to room temperature and the solvent was removed under vacuum. The solid was dissolved in water (10 mL) and filtered. Few droplets of hexafluorophosphoric acid were then added to the aqueous solution to allow precipitation. The solid was then collected by filtration on a Büchner funnel and washed with cold water, ethanol, and ether. The red/orange solid was recovered and dried in an oven at 50°C for 5 hours. ^{1}H-NMR (300 MHz, CD_3CN): δ_H 8.51 (4H, d), 8.38 (2H, s), 8.06 (4H, dd), 7.75 (4H, dd), 7.54 (2H, d), 7.41 (4H, dd), 7.24 (2H, d), 2.55 (6H, s).

Tris(4,4'-dimethyl-2,2'-bipyridine)ruthenium(II) dihexafluorophosphate (**Ru3**). 1 equivalent of dichloro(*p*-cymene)ruthenium(II) dimer (167 mg, 0.33 mmol) was dissolved in 30 mL DMF, 6 equivalents of 4,4'-dimethyl-2,2'-bipyridine (301 mg, 1.95 mmol) were then added and the mixture was heated under reflux for 5 hours under continuous stirring. The reaction was followed by thin-layer chromatography (silica, 9/1 ethyl acetate/dichloromethane) and by UV-Vis absorption (monitoring the formation of the MLCT absorption at ca. 450 nm). The mixture was cooled to room temperature and the solvent was removed under vacuum. The solid was dissolved in water (10 mL) and filtered. Few droplets of hexafluorophosphoric acid were then added to the aqueous solution to allow precipitation. The solid was then collected by filtration on a Büchner funnel and washed with cold water, ethanol, and ether. The red/orange solid was recovered and dried in an oven at 50°C for 5 hours. ^{1}H-NMR (300 MHz, CD_3CN): δ_H 8.35 (6H, d), 7.54 (6H, dd), 7.22 (6H, dd), 2.54 (18H, s).

Tris(4,4'-di*tert*butyl-2,2'-bipyridine) ruthenium(II) dihexafluorophosphate (**Ru4**). 1 equivalent of dichloro(*p*-cymene)ruthenium(II) dimer (187 mg, 0.37 mmol) was dissolved in 30 mL DMF, 6 equivalents of 4,4'-di*tert*butyl-2,2'-bipyridine (590 mg, 2.22 mmol) were then added and the mixture was heated under reflux for 7 hours under continuous stirring. The reaction was followed by thin-layer chromatography (silica, 9/1 ethyl acetate/dichloromethane) and by UV-Vis absorption (monitoring the formation of the MLCT absorption at ca. 450 nm). The mixture was cooled to room temperature and the solvent was removed under vacuum. The solid was dissolved in water (10 mL) and filtered. Few droplets of hexafluorophosphoric acid were then added to the aqueous solution to allow precipitation. The solid was then collected by filtration on a Büchner funnel and washed with cold water, ethanol, and ether. The red/orange solid was recovered and dried in an oven at 50°C for 5 hours. ^{1}H-NMR (300 MHz, CD_3CN): δ_H 8.49 (6H, d), 7.56 (6H, dd), 7.41 (6H, dd), 2.19 (54H, s).

Bis(dimethylglioximate)pyridine cobalt(III) chloride (**CoDMG**). $CoCl_2 \cdot 6H_2O$ (2 g, 8.4 mmol) and $dmgH_2$ (dimethylglioxime, 2.14 g, 18.5 mmol) were dissolved in 95% ethanol (30 mL), and the solution was heated to 70°C. Pyridine (1.36 mL, 16.8 mmol) was then added to the reaction mixture and the solution was stirred for 1 h at 70°C. After cooling to room temperature, a stream of air was blown through the solution for 30 min and a brown precipitate was formed. Brown crystals were collected by filtration on a Büchner funnel and washed with cold ethanol (5 mL), water (5 mL), and then with diethyl ether (10 mL). The solid was then dried at room temperature. The crude product was recrystallized from acetonitrile. ^{1}H-NMR (300 MHz, CD_3CN): δ_H 18.56 (2H, s), 8.14 (2H, dd), 7.80 (1H, dd), 7.32 (2H, dd), 2.33 (12H, s).

Apparatus and procedures.

Cyclic voltammetry (CV) and differential pulse voltammetry (DPV) measurements were carried out on a PC-interfaced Eco Chemie Autolab/Pgstat 30 Potentiostat. Argon-purged sample solutions in 50/50 water/acetonitrile, containing 0.1 M $LiClO_4$, were used. A conventional three-electrode cell assembly was adopted: a saturated calomel electrode (SCE Amel) and a platinum electrode, both separated from test solution by a glass frit, were used as reference and counter electrodes, respectively; a glassy carbon electrode was used as the working electrode. Half-wave potentials ($E_{1/2}$) for reversible processes have been calculated as $E_{1/2} = (E_{cp} + E_{ap})/2$ in the CV, where E_{cp} and E_{ap} are the cathodic and anodic peak potentials, respectively, or as $E_{1/2} = E_p + \Delta E/2$ in the DPV, where E_p and ΔE are the peak potential and the pulse width, respectively.

UV-Vis absorption spectra were recorded on a Jasco V-570 UV/Vis/NIR spectrophotometer. Emission spectra were taken on a Horiba-Jobin Yvon Fluoromax-2 spectrofluorimeter,

equipped with a Hamamatsu R3896 tube. Nanosecond transient absorption and time-resolved emission measurements were performed with a custom laser spectrometer comprised of a Continuum Surelite II Nd:YAG laser (FWHM 6 - 8ns) with frequency doubled, (532 nm, 330 mJ) or tripled, (355 nm, 160 mJ) option, an Applied Photophysics xenon light source including a mod. 720 150 W lamp housing, a mod. 620 power controlled lamp supply and a mod. 03 - 102 arc lamp pulser. Laser excitation was provided at 90° with respect to the white light probe beam. Light transmitted by the sample was focused onto the entrance slit of a 300 mm focal length Acton SpectraPro 2300i triple grating, flat field, double exit monochromator equipped with a photomultiplier detector (Hamamatsu R3896). Signals from the photomultiplier (kinetic traces) were processed by means of a LeCroy 9360 (600 MHz, 5 Gs/s) digital oscilloscope.

The hydrogen evolution experiments were carried out upon continuous visible light irradiation with a 175 W xenon arc-lamp (*CERMAX PE175BFA*) of a reactor containing the solution (a 10 mm pathlength pyrex glass cuvette with head space obtained from a round-bottom flask). A cut-off filter at 400 nm and a hot mirror (IR filtering) have been used to provide the useful wavelength range (400-800 nm). The reactor is placed at a distance of 20 cm from the irradiation source and the light beam is completely focused on the reactor (all the solution is irradiated during the experiment). The measuring cell is sealed during the photoreaction: the head to which cell is attached has indeed four ports, closed with Swagelok® connections, two of them are part of a closed loop involving GC gas inlet and sample vent in order to analyze head space content without any appreciable gas consumption, and the other two are for the degassing procedure (input and output). The gas phase of the reaction vessel was analyzed on an Agilent Technologies 490 microGC equipped with a 5 Å molecular sieve column (10 m), a thermal conductivity detector, and using Ar as carrier gas. 5 mL from the headspace of the reactor are sampled by the internal GC pump and 200 nL are injected in the column maintained at 60°C for separation and detection of gases. The unused gas sample is then reintroduced in the reactor in order to minimize its consumption along the whole photolysis. The amount of hydrogen was quantified through the external calibration method. This procedure was performed, prior to analysis, through a galvanostatic (typically 1 mA) electrolysis of a 0.1 M H_2SO_4 solution in an analogous cell (same volume) equipped with two Pt wires sealed in the glass at the bottom of the cell. A 100% faradaic efficiency was assumed leading to a linear correlation between the amount of H_2 evolved at the cathode and the electrolysis time. In a typical photcatalytic experiment, samples of 5 mL were prepared in 20 mL scintillation vials starting from the sensitizer (0.5 mL from a 5 mM mother solution in acetonitrile), and further adding **CoDMG** (65 μL from 7.6 mM mother solution in acetonitrile), acetonitrile (1.935 mL), water (2.5 mL), and finally ascorbic acid (as solid). The pH was adjusted at 5 with NaOH upon addition of few droplets from a 5 M stock solution. The solution was then put in the reactor, degassed by bubbling Ar for 20 min, and thermostated at 15°C. The cell was then irradiated and the solution continually stirred during the photolysis. The gas phase of the reaction was analyzed through GC and the amount of hydrogen quantified.

Acknowledgements

The authors gratefully acknowledge Prof. Franco Scandola for fruitful discussions. Financial support from the Italian MIUR (FIRB RBAP11C58Y "NanoSolar", PRIN 2010 "Hi-Phuture") and COST action CM1202 "PERSPECT-H2O" is gratefully acknowledged.

Notes and references

‡ Quantum yields have been calculated taking **Ru1** as actinometer ($\Delta\varepsilon$ = −10,600 $M^{-1}cm^{-1}$ at 450 nm and Φ = 1 for ^{3}***Ru1**),[17] then considering the maximum ΔOD value in the kinetic trace and using a molar extinction coefficient of $\Delta\varepsilon$ = 9,000 $M^{-1}cm^{-1}$ at λ = 500 nm[16] (assumed to be appreciably similar throughout the **Ru1-4** series).

§ This is very likely an artifact, arising from the slower rate of transient formation in **Ru3** and **Ru4**. In these cases, with transient decay taking place in a comparable time scale, the maxima in the kinetic plots do not feature full transient accumulation.

§§ Ascorbate behaves as a sacrificial electron donor provided that an electron transfer from the reduced sensitizer to a secondary acceptor (e.g., the catalyst) occurs in competition with charge recombination. This process would permanently yield the oxidized species of the ascorbate which undergoes a disproportionation reaction (bimolecular rate of k = ~8 × 10^7 $M^{-1}s^{-1}$) to give ascorbic acid and dehydroascorbic acid.[19]

¶ The optical path to be used to correlate the ΔOD signal and the concentration of reduced sensitizer, according to the Lambert-Beer law, is herein better defined as a correction parameter which accounts for the ratio between the volume of solution probed by the analyzing beam and that excited by the laser pulse; see, e.g., ref. 20.

‖ This result seems to be a general feature of photochemical systems for hydrogen evolution involving ascorbic acid as the sacrificial donor and cobaloxime or even more generally cobalt(III) molecular complexes as the hydrogen evolving catalysts. Thus care has to be taken when investigating photocatalytic mechanisms or photoinduced electron transfer kinetics involving these molecular components.

Under these conditions additional turnover limiting factors can be disregarded, including the consumption of the sacrificial donor (< 20%) and strong pH variations (final pH is ca 6 in all cases, where the **CoDMG** is known to be still active for proton reduction, see, e.g., ref. 11h).

1 (a) J. H. Alstrum-Acevedo, M. K. Brennaman and T. J. Meyer, *Inorg. Chem.* 2005, **44**, 6802. (b) N. S. Lewis and D. G. Nocera, *Proc. Natl. Acad. Sci. U.S.A.* 2006, **103**, 15729. (c) R. Eisenberg and H. B. Gray, *Inorg. Chem.* 2008, **47**, 1697. (d) D. G. Nocera, *Inorg. Chem.* 2009, **48**, 10001. (e) H. B. Gray, *Nat. Chem.* 2009, **1**, 7. (f) N. Armaroli, V. Balzani and N. Serpone, *Powering Planet Earth: Energy Solutions for the Future*, Wiley, New York, 2012. (g) D. Gust, T. A. Moore and A. L. Moore, *Faraday Disc.* 2012, **155**, 9. (h) J. R. McKone, N. S. Lewis and H. B. Gray, *Chem. Mater.* 2014, **26**, 407.

2 J. R. McKone, S. C. Marinescu, B. S. Brunschwig, J. R. Winkler and H. B. Gray, *Chem. Sci.* 2014, **5**, 865.

3 (a) T. S. Teets and D. G. Nocera, *Chem. Commun.* 2011, **47**, 9268. (b) W. T. Eckenhoff and R. Eisenberg, *Dalton Trans.*

2012, **41**, 13004. (c) E. S. Andreiadis, M. Chavarot-Kerlidou, M. Fontecave and V. Artero, *Photochem. Photobio.* 2011, **87**, 946.
4 (a) W. T. Eckenhoff, W. R. McNamara, P. Du and R. Eisenberg, *Biochim. Biophys. Acta* 2013, **1827**, 958. (b) K. Ladomenou, M. Natali, E. Iengo, G. Charalampidis, F. Scandola and A. G. Coutsolelos, *Coord. Chem. Rev.* 2015, **304-305**, 38.
5 (a) Y. Sun, J. Sun, J. R. Long, P. Yang and C. J. Chang, *Chem. Sci.* 2013, **4**, 118. (b) M. Nippe, R. S. Khnayzer, J. A. Panetier, D. Z. Zee, B. S. Olaiya, M. Head-Gordon, C. J. Chang, F. N. Castellano and J. R. Long, *Chem. Sci.* 2013, **4**, 3934. (c) R. S. Khnayzer, V. A. Thoi, M. Nippe, A. E. King, J. W. Jurss, K. A. El Roz, J. R. Long, C. J. Chang and F. N. Castellano, *Energy Environ. Sci.* 2014, **7**, 1477. (d) W. M. Singh, M. Mirmohades, R. T. Jane, T. A. White, L. Hammarström, A. Thapper, R. Lomoth and S. Ott, *Chem. Commun.* 2013, **49**, 8638. (e) L. Tong, R. Zong and R. P. Thummel, *J. Am. Chem. Soc.* 2014, **136**, 4881. (f) E. Deponti, A. Luisa, M. Natali, E. Iengo and F. Scandola, *Dalton Trans.* 2014, **43**, 16345. (g) J. W. Jurss, R. S. Khnayzer, J. A. Panetier, K. A. El Roz, E. M. Nichols, M. Head-Gordon, J. R. Long, F. N. Castellano and C. J. Chang, *Chem. Sci.* 2015, **6**, 4954.
6 (a) W. M. Singh, T. Baine, S. Kudo, S. Tian, X. A. N. Ma, H. Zhou, N. J. De Yonker, T. C. Pham, J. C. Bollinger, D. L. Baker, B. Yan, C. E. Webster and X. Zhao, *Angew. Chem. Int. Ed.* 2012, **51**, 5941. (b) M. Vennampalli, G. Liang, L. Katta, C. E. Webster and X. Zhao, *Inorg. Chem.* 2014, **53**, 10094.
7 (a) W. R. McNamara, Z. Han, P. J. Alperin, W. W. Brennessel, P. L. Holland and R. Eisenberg, *J. Am. Chem. Soc.* 2011, **133**, 15368. (b) W. R. McNamara, Z. Han, C.-J. Yin, W. W. Brennessel, P. L. Holland and R. Eisenberg, *Proc. Natl. Acad. Sci. U.S.A.* 2012, **109**, 15594.
8 M. Natali, A. Luisa, E. Iengo and F. Scandola, *Chem. Commun.* 2014, **50**, 1842.
9 A. Juris, V. Balzani, F. Barigelletti, S. Campagna, P. Belser and A. Von Zelewsky, *Coord. Chem. Rev.* 1988, **84**, 85.
10 (a) S. Losse, J. G. Vos and S. Rau, *Coord. Chem. Rev.* 2010, **254**, 2492. (b) R. Staehle, S. Losse, M. R. Filipovic, I. Ivanovic-Burmazovic, J. G. Vos and S. Rau, *ChemPlusChem* 2014, **79**, 1614.
11 (a) P. Du, K. Knowles and R. Eisenberg, *J. Am. Chem. Soc.* 2008, **130**, 12576. (b) A. Fihri, V. Artero, M. Razavet, C. Baffert, W. Leibl and M. Fontecave, *Angew. Chem., Int. Ed.* 2008, **47**, 564. (c) T. M. McCormick, B. D. Calitree, A. Orchard, N. D. Kraut, F. V. Bright, M. R. Detty and R. Eisenberg, *J. Am. Chem. Soc.* 2010, **132**, 15480. (d) J. L. Dempsey, J. R. Winkler and H. B. Gray, *J. Am. Chem. Soc.* 2010, **132**, 1060. (e) J. L. Dempsey, B. S. Brunschwig, J. R. Winkler and H. B. Gray, *Acc. Chem. Res.* 2009, **42**, 1995. (f) B. Prost, M. Guttentag, A. Rodenberg, P. Hamm and R. Alberto, *Inorg. Chem.* 2011, **50**, 3404. (g) F. Lakadamyali, A. Reynal, M. Kato, J. R. Durrant and E. Reisner, *Chem. Eur. J.* 2012, **18**, 15464. (h) M. Natali, R. Argazzi, C. Chiorboli, E. Iengo and F. Scandola, *Chem. Eur. J.* 2013, **19**, 9261. (i) R. S. Khnayzer, C. E. McCusker, B. S. Olaiya and F. N. Castellano, *J. Am. Chem. Soc.* 2013, **135**, 14068. (l) E. Rousset, D. Chartrand, I. Ciofini, V. Marvaud and G. S. Hanan, *Chem. Commun.* 2015, **51**, 9261.
12 (a) M. T. Indelli, C. A. Bignozzi, F. Scandola and J. P. Collin, *Inorg. Chem.* 1998, **37**, 6084. (b) M. T. Indelli, M. Ghirotti, A. Prodi, C. Chiorboli, F. Scandola, N. D. McClenaghan, F. Puntoriero and S. Campagna, *Inorg. Chem.* 2003, **42**, 5489.
13 C. Chiorboli, M. T. Indelli, M. A. Rampi Scandola and F. Scandola, *J. Phys. Chem.* 1988, **92**, 156.
14 M. Z. Hoffmann, F. Bolletta, L. Moggi and G. L. Hug, *J. Phys. Chem. Ref. Data* 1989, **18**, 219.
15 D. Sandrini, M. Maestri, P. Belser, A. Von Zelewski and V. Balzani, *J. Phys. Chem.* 1985, **89**, 3675.
16 (a) C. Creutz and N. Sutin, *J. Am. Chem. Soc.* 1976, **98**, 6384. (b) L. A. Kelly and M. A. J. Rodgers, *J. Phys. Chem.* 1994, **98**, 6377.
17 C. Creutz, M. Chou, T. L. Netzel, M. Okumura and N. Sutin, *J. Am. Chem. Soc.* 1980, **102**, 1309.
18 B. Shan, T. Baine, X. A. N. Ma, X. Zhao and R. H. Schmehl, *Inorg. Chem.* 2013, **52**, 4853.
19 (a) B. H. J. Bielski, D. A. Comstock and R. A. Bowen, *J. Am. Chem. Soc.* 1971, **93**, 5624. (b) C. Creutz, N. Sutin and B. S. Brunschwig, *J. Am. Chem. Soc.* 1979, **101**, 1298.
20 M. Natali, M. Orlandi, S. Berardi, S. Campagna, M. Bonchio, A. Sartorel and F. Scandola, *Inorg. Chem.* 2012, **51**, 7324.
21 S. Yamabe, N. Tsuchida, S. Yamazaki and S. Sakaki, *Org. Biomol. Chem.* 2015, **13**, 4002.
22 (a) M. Natali, M. Orlandi, C. Chiorboli, E. Iengo, V. Bertolasi and F. Scandola, *Photochem. Photobio. Sci.* 2013, **12**, 1749. (b) J. C. Manton, C. Long, J. G. Vos and M. T. Pryce, *Dalton Trans.* 2014, **43**, 3576.
23 E. A. Juban, A. L. Smeigh, J. E. Monat and J. K. McCusker, *Coord. Chem. Rev.* 2006, **250**, 1783.
24 (a) P. Du, J. Schneider, G. Luo, W. W. Brennessel and R: Eisenberg, *Inorg. Chem.* 2009, **48**, 4952. (b) O. Pantani, E. Anxolabéhère-Mallart, A. Aukauloo and P. Millet, *Electrochem. Comm.* 2007, **9**, 54.
25 (a) A. Bhattacharjee, E. S. Andreiadis, M. Chavarot-Kerlidou, M. Fontecave, M. J. Field and V. Artero, *Chem. Eur. J.* 2013, **19**, 15166. (b) B. H. Solis, Y. Yu and S. Hammes-Schiffer, *Inorg. Chem.* 2013, **52**, 6994.
26 (a) C. Creutz, H. A. Schwarz, J. F. Wishart, E. Fujita and N. Sutin, *J. Am. Chem. Soc.* 1991, **113**, 3361. (b) A. Lewandowska-Andralojc, T. Baine, X. Zhao, J. T. Muckermann, E. Fujita and D. E. Polyansky, *Inorg. Chem.* 2015, **54**, 4310.
27 C. V. Krishnan and N. Sutin, *J. Am. Chem. Soc.* 1981, **103**, 2141.
28 N. Armaroli, G. Accorsi, D. Felder and J.-F. Nierengarten, *Chem. Eur. J.* 2002, **8**, 2314.
29 N. H. Damrauer, T. R. Boussie, M. Devenney and J. K. McCusker, *J. Am. Chem. Soc.* 1997, **119**, 9253.
30 (a) A. Juris, V. Balzani, P. Belser and A. Von Zelewsky, *Helv. Chim. Acta* 1981, **64**, 2175. (b) A. Juris, F. Barigelletti, V. Balzani, P. Belser and A. Von Zelewsky, *Isr. J. Chem.* 1982, **22**, 87.
31 G. N. Schrauzer, *Inorg. Synth.* 1968, **11**, 61.